Chinese Chemical Letters 34 (2023) 108801

Contents lists available at ScienceDirect

Chinese Chemical Letters

journal homepage: www.elsevier.com/locate/cclet

Molecular confined synthesis of magnetic CoO_x/Co/C hybrid catalyst for photocatalytic water oxidation and CO_2 reduction

Rui Li[a,1], Chenchen Zhang[a,1], Kejia You[a], Bonan Li[a], Wei Bu[a], Xiangyu Meng[a,c,*], Baochun Ma[a], Yong Ding[a,b,*]

[a] State Key Laboratory of Applied Organic Chemistry, Key Laboratory of Advanced Catalysis of Gansu Province, College of Chemistry and Chemical Engineering, Lanzhou University, Lanzhou 730000, China
[b] State Key Laboratory for Oxo Synthesis and Selective Oxidation, Lanzhou Institute of Chemical Physics, Chinese Academy of Sciences, Lanzhou 730000, China
[c] Henan Provincial Key Laboratory of Nanocomposites and Applications, Institute of Nanostructured Functional Materials, Huanghe Science and Technology College, Zhengzhou 450006, China

ARTICLE INFO

Article history:
Received 18 May 2023
Revised 11 July 2023
Accepted 12 July 2023
Available online 14 July 2023

Keywords:
CoO_x/Co/C
Water oxidation
CO_2 reduction
Photocatalyst
Photosensitizer

ABSTRACT

Photosynthesis [$6CO_2 + 12H_2O \rightarrow (CH_2O)_6 + 6O_2 + 6H_2O$] in nature contains a light reaction process for oxygen evolution and a dark reaction process for carbon dioxide (CO_2) reduction to carbohydrates, which is of great significance for the survival of living matter. Therefore, for simulating photosynthesis, it is desirable to design and fabricate a bifunctional catalyst for promoting photocatalytic water oxidation and CO_2 reduction performances. Herein, a molecular confined synthesis strategy is reasonably proposed and applied, that is the bifunctional CoO_x/Co/C-T (T = 700, 800 and 900 °C) photocatalysts prepared by the pyrolysis of molecular Co-EDTA under N_2 and air atmosphere in turn. Among the prepared photocatalysts, the CoO_x/Co/C-800 shows the best photocatalytic water oxidation activity with an oxygen yield of 51.2%. In addition, for CO_2 reduction reaction, the CO evolution rate of 12.6 μmol/h and selectivity of 75% can be achieved over this catalyst. The improved photocatalytic activities are attributed to the rapid electron transfer between the photosensitizer and the catalyst, which is strongly supported by the current density-voltage (*j-V*), steady-state and time-resolved photoluminescence spectra (PL). Overall, this work provides a reference for the preparation and optimization of photocatalysts with the capacity for water oxidation and CO_2 reduction reactions.

The use of fossil fuels has brought about increasingly serious problems of greenhouse effect and energy shortage [1,2]. Mimicking natural photosynthesis for developing clean and renewable energy sources is one of the efficient and promising methods to deal with these problems. In biological systems, photosynthesis [$6CO_2 + 12H_2O \rightarrow (CH_2O)_6 + 6O_2 + 6H_2O$] contains a light reaction process for oxygen evolution and a dark reaction process for carbon dioxide (CO_2) reduction to carbohydrates [3,4]. However, both reactions are uphill processes and need external solar energy to drive [5,6]. Therefore, it is highly desirable in artificial photosynthesis to develop the corresponding catalysts to reduce the energy barriers of reaction.

Exploration for the first transition metal-based catalysts has been pursued vigorously, in which their unfilled d orbit structure is favorable in donating and capturing electrons during reaction [7–9]. Especially, lots of homogeneous and heterogeneous Co-based compounds for photocatalytic CO_2 reduction and water oxidation reaction have been investigated vigorously [10–15]. Recently, due to the unique conductivity and electrochemical properties, carbon-based catalysts such as carbon nanotubes, carbon quantum dots, graphene and their composite materials have been widely adopted for water oxidation and carbon dioxide reduction reaction [16,17]. Therefore, some metal nanoparticles coated with carbon layers are used for photocatalytic water oxidation, hydrogen evolution and CO_2 reduction, where Co-based samples exhibited remarkable catalytic activity [18,19]. In these complex catalysts, the metal nanoparticles have good conductivity due to the existence of metallic bonding, while the coated carbon layers further enhance the conductivity and stability of the catalyst. Because of the synergy between carbon layers and metal nanoparticles, these hybrid

* Corresponding authors.
E-mail addresses: 202206132@hhstu.edu.cn (X. Meng), dingyong1@lzu.edu.cn (Y. Ding).
[1] These authors contributed equally to this work.

https://doi.org/10.1016/j.cclet.2023.108801
1001-8417/

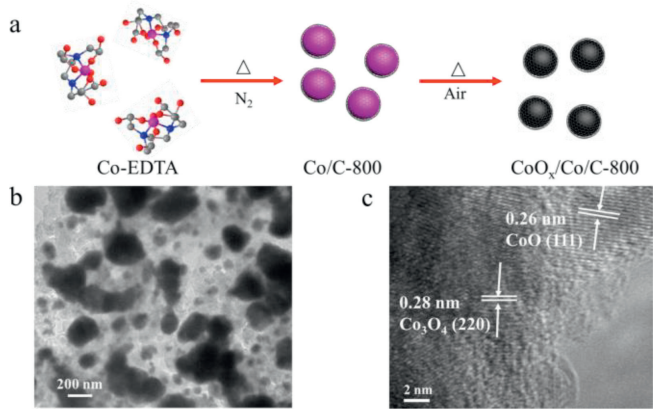

Fig. 1. (a) Illustration of the synthesis of catalysts, (b) transmission electron microscopy (TEM) and (c) high-resolution transmission electron microscopy (HRTEM) images of CoO_x/Co/C-800.

materials usually possess good activity as catalysts or cocatalysts for photocatalytic reaction [20,21]. In the past few years, MOFs were often served as precursors to fabricate carbon-coated metal materials, however, it suffers from the synthesis processes complicated and inconvenient to popularization and application [22,23].

Inspired by the above, a series of carbon-coated cobalt-based catalysts (denoted as Co/C-T and CoO_x/Co/C-T) were obtained through a simple one-step or two-step calcination of Co-EDTA complex in this work, which were used for visible light driven water oxidation and CO_2 reduction reactions. The oxygen evolution activity of CoO_x/Co/C-T obtained from a two-step calcination process under N_2 and air atmosphere in sequence was better than that of Co/C-T through a one-step calcination process in N_2 atmosphere. Furthermore, the CoO_x/Co/C-T exhibited poorer hydrogen evolution performance, which resulted in a higher photocatalytic CO selectivity than that of Co/C-T thereby. Overall, this work provides a new insight for the preparation and optimization of catalysts with the capacity of oxygen production and CO_2 reduction.

The CoO_x/Co/C-T samples were prepared by a two-step calcination of Co-EDTA as shown in Fig. 1a. In the first step, Co/C-T catalysts were obtained through calcinating Co-EDTA under N_2 atmosphere. A 30.5% weight loss occurs between 336.0 and 392.2 °C in the TG curve (Fig. S2 in Supporting information), corresponding to a carbonization process of the complex. Cobalt ions in the Co-EDTA are thermally reduced by the produced reducing gas, which results in the products containing cobalt metal and carbon. After 392.2 °C, there is still a slow weight loss, which may result in a difference of carbon content in Co/C-700, 800, 900. In the second step, Co/C-T was further annealed in air to afford new active sites CoO_x on the surface of Co/C-T. As shown in Fig. S3 (Supporting information), these catalysts all have magnetic capacity due to the existence of metallic Co, which is helpful to the recovery of the hybrid catalyst.

The morphology of CoO_x/Co/C-800 was characterized by TEM and presented in Figs. 1b and c. Co particles are surrounded by carbon layers. HRTEM image shows clear lattice fringes of 0.28 nm corresponding to the (220) crystal planes of Co_3O_4. The lattice spacing of 0.26 nm corresponds to the (111) crystal plane of CoO. The cobalt particles are tightly bound to the carbon layer, which is beneficial for electron transfer.

The crystalline structure of catalysts was investigated through powder X-ray diffraction (XRD). In Fig. 2a, there are three obvious diffraction peaks in the XRD patterns of Co/C-800 and CoOx/Co/C-800 samples locating at 44.3°, 51.8° and 76°, which are corresponding to (111), (200) and (220) planes of the face-centered (fcc) metallic Co phase (PDF#15–0806), respectively. There are no

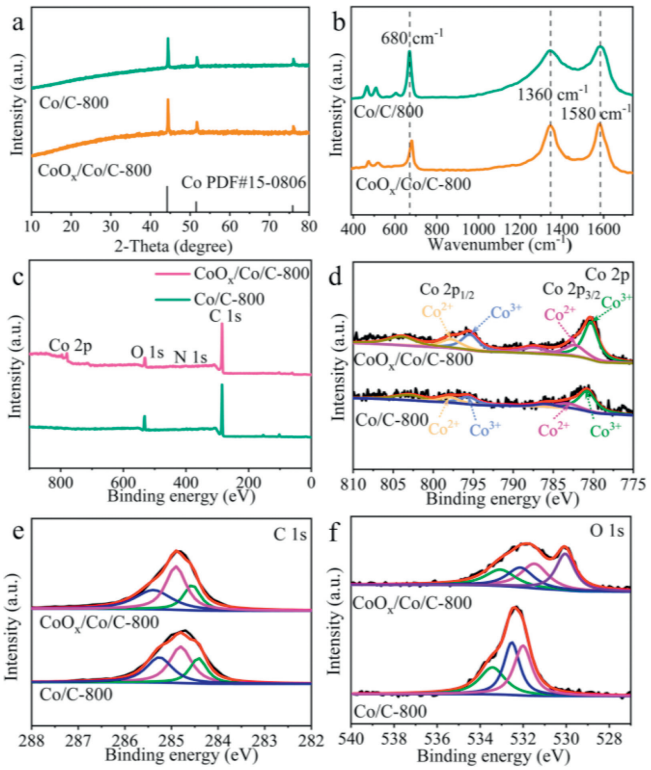

Fig. 2. (a) XRD patterns, (b) Raman spectra of Co/C-800 and CoO_x/Co/C-800. (c) Survey and (d-f) high-resolution Co 2p, C 1s and O 1s XPS spectra of Co/C-800 and CoO_x/Co/C-800.

diffraction peaks of C composition and cobalt oxide appearing in the XRD patterns of catalysts, indicating carbon layers and CoO_x may be highly dispersed on the surface [24]. The XRD patterns of other catalysts are shown in Fig. S4 (Supporting information), in which the Co/C-700/900 and CoO_x/Co/C-700/900 also show the diffraction peaks of face-centered (fcc) metallic Co phase only.

The Raman spectra of Co/C-800 and CoO_x/Co/C-800 were obtained with an excitation wavelength of 532 nm shown in Fig. 2b. The peaks at 1580 and 1360 cm^{-1} are corresponding to G peak and D peak of the carbon layers, and catalysts have high conductivity due to the fact that D and G peaks have similar intensity, whose high conductivity is beneficial for electron transfer [25]. The peaks at 680, 519 and 473 cm^{-1} of CoO_x/Co/C-800 correspond to vibration modes of A_{1g}, F_{2g} and E_g, resulting from Co-O bond stretching vibration at Co^{3+} of octahedral coordination and O-Co-O bending vibration of Co^{2+} of tetrahedral coordination [26]. Compared to Co/C-800, the peaks in CoO_x/Co/C-800 have a slight shift, which may be caused by the increasing content of CoO_x of sample [27].

The surface chemical compositions and valence states of the catalysts were detected by X-ray photoelectron spectroscopy (XPS). XPS survey spectra of Co/C-800 and CoO_x/Co/C-800 exhibit the presence of four elements C, N, Co and O on the surface (Figs. 2c-f). For CoO_x/Co/C-800, $2p_{3/2}$ and $2p_{1/2}$ peaks of Co^{2+} and Co^{3+} are located at 782.5/797.8 and 780.4/795.4 eV, respectively, and the corresponding satellite peaks are at 787.5 and 803.9 eV. The Co $2p_{3/2}$–$2p_{1/2}$ spin-orbit splitting (ΔE) is 15.3 eV for CoO and 15.0 eV for Co_3O_4, which further indicates that the cobalt oxide in prepared material is a mixture of the two forms [22]. For Co/C-800, the intensity of peaks for Co is lower than that of CoO_x/Co/C-800 and the reason is maybe that more carbon layers cover on the surface of former. The C 1s peaks are similar for both Co/C-800 and CoO_x/Co/C-800, while there is a new peak at 530.1 eV appears for CoO_x/Co/C-800 in O 1s spectra, which is ascribed to lattice oxy-

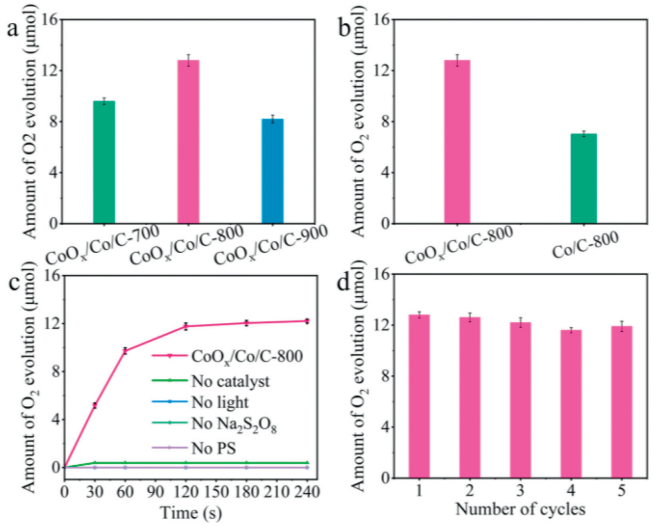

Fig. 3. Photocatalytic oxygen evolution amount of (a) CoO_x/Co/C-700, CoO_x/Co/C-800 and CoO_x/Co/C-900, (b) Co/C-800 and CoO_x/Co/C-800. (c) Kinetic curves under different conditions. (d) Recycle stability experiments of CoO_x/Co/C-800.

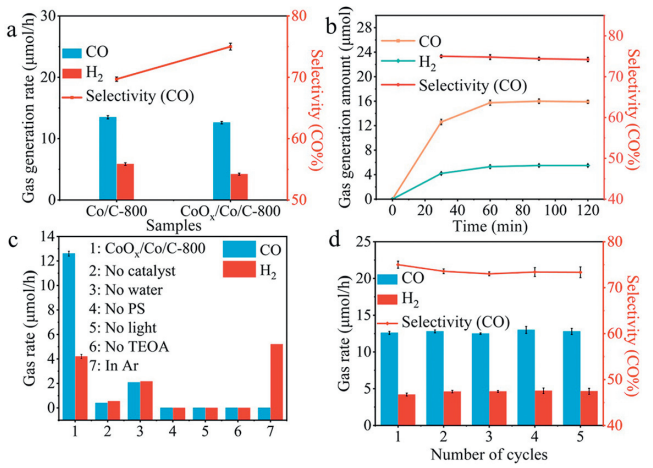

Fig. 4. (a) Photocatalytic gas generation rates. (b) Kinetic curves for gas evolution amount of CoO_x/Co/C-800. (c, d) Single variable control experiments and recycling experiments for photocatalytic CO_2 reduction over CoO_x/Co/C-800.

gen [28]. Furthermore, the IR peaks at 668 and 587 cm^{-1} which are assigned to lattice Co-O vibration of Co_3O_4 strongly support the existence of CoO_x on the surface of CoO_x/Co/C-800 (Fig. S5 in Supporting information) [29].

The optimization of the conditions for photocatalytic oxygen production reaction is shown in Figs. 3a and b. The evolution amount of oxygen over samples CoO_x/Co/C-700, CoO_x/Co/C-800 and CoO_x/Co/C-900 are 9.6, 12.8 and 8.2 μmol, with oxygen yields of 38.4%, 51.2% and 32.8%, respectively. Among them, CoO_x/Co/C-800 has the best catalytic activity. In Fig. S6 (Supporting information), the amount of oxygen evolution over 0.5, 1.0 and 2.0 mg CoO_x/Co/C-800 as photocatalysts are 10.7, 12.8 and 9.9 μmol, respectively. Then, 1.0 mg CoO_x/Co/C-800 was selected to optimize pH for oxygen evolution and the pH for highest activity is 8.5. High pH is conducive to the progress of the oxygen evolution reaction, but too high pH will promote the decomposition of photosensitizer, reducing the reaction activity [30]. CoO_x/Co/C-800 obtained by two-step calcination shows better activity with 12.8 μmol O_2 generated, which is 1.8 times higher than that of Co/C-800 (7.0 μmol). The improvement of oxygen evolution activity of CoO_x/Co/C-800 may be attributed to the presence of CoO_x on the surface, which makes it easier to generate hypervalent intermediate species to drive oxygen evolution [31]. According to ^{18}O isotope labeling experiment, all oxygen comes from water (Fig. S7 in Supporting information). The photocatalytic activities of CoO_x/Co/C-700/900 and Co/C-700/900 are listed in Fig. S8 (Supporting information), suggesting that CoO_x/Co/C-T samples obtained by two-step calcination have a better activity than corresponding Co/C-T. It can be concluded that the calcination process in air is helpful for promoting activity in this photocatalytic oxygen evolution system.

The single variable control experiments and oxygen evolution dynamics were investigated (Fig. 3c). The amount of oxygen increases linearly during 0–60 s and the reaction rate decreases at 60–90 s, then reaches a plateau after 120 s. The stop of oxygen evolution could be ascribed to the inactivation of photosensitizer and the depletion of sacrificial reagent [32]. For oxygen evolution, photosensitizer (PS), sacrificial reagent $Na_2S_2O_8$, catalyst and light are all required. In the absence of catalyst CoO_x/Co/C-800, the photosensitizer drives water oxidation with poor activity of oxygen production (0.4 μmol), and the addition of catalyst greatly promotes the reaction efficiency. After five cycles, the amount of oxygen evolution is almost unchanged, which means the catalyst structure remains stable during the reaction time (Fig. 3d).

The photocatalytic CO_2 reduction reaction was carried out under classical conditions with $[Ru(bpy)_3]Cl_2$ as photosensitizer and triethanolamine (TEOA) as sacrificial reagent. The gas product of photocatalytic carbon dioxide reduction reaction is only CO, and there is no liquid product (Figs. S9 and S10 in Supporting information). As shown in Fig. 4a, the CO production rate catalyzed by CoO_x/Co/C-800 is 12.6 μmol/h, slightly lower than that of Co/C-800 (13.5 μmol/h), but the CO selectivity of CoO_x/Co/C-800 is 75% and that of Co/C-800 is 69%. The higher CO selectivity of CoO_x/Co/C-800 is due to the increasing content of CoO_x on the surface of sample. In order to further compare the photocatalytic hydrogen production capacity of CoO_x/Co/C-800 and Co/C-800, hydrogen production experiments were conducted in the same reaction condition (7.5 mg photosensitizer, 6 mL reaction solution, except argon gas replacing CO_2 to bubble in the reaction bottle). As shown in Fig. S11 (Supporting information), the hydrogen production activity of CoO_x/Co/C-800 (6.2 μmol) is lower than that of Co/C-800 (9.7 μmol), suggesting the CoO_x is not conductive to photocatalytic hydrogen evolution. The photocatalytic CO_2 reduction activity of CoO_x/Co/C-700/900 and Co/C-700/900 perform similar trend law as those of CoO_x/Co/C-800 and Co/C-800 (Fig. S12 in Supporting information) [33,34]. Therefore, the introduction of active species CoO_x to inhibit H_2 generation is one of the methods to improve the CO selectivity. In Fig. 4b, gas production rates gradually decrease during a two hours kinetic experiment due to the $[Ru(bpy)_3]Cl_2$ being unstable under alkaline conditions [35]. To investigate the necessary conditions for CO evolution, single variable control experiments were conducted (Fig. 4c). For CO_2 reduction reaction, photosensitizer, sacrificial reagent and light are indispensable. The experiment in Ar and the isotopic $^{13}CO_2$ experiment suggest the produced CO is derived from CO_2 (Fig. S13 in Supporting information). Without adding catalyst, only trace CO and H_2 are observed. It is worth noting that the conversion of CO_2 and selectivity to CO are almost constant (Fig. 4d), revealing the CoO_x/Co/C-800 as a photocatalyst has good stability for CO_2 reduction reaction.

In order to check the stability of the catalyst, Raman, XRD and IR spectra of the recovered catalyst and the fresh one were performed (Figs. S14-S17 in Supporting information). The similar spectra of CoO_x/Co/C-800 before and after photocatalytic water oxidation and CO_2 reduction reaction suggest that this catalyst has good stability during photocatalytic reactions [36,37].

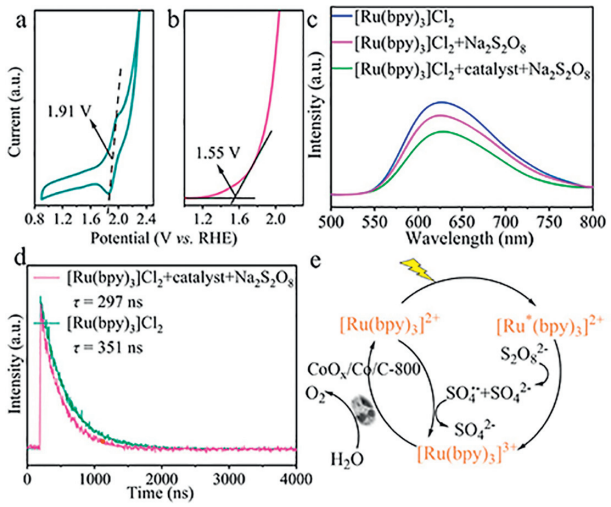

Fig. 5. (a) CV curve of $[Ru(bpy)_3]Cl_2$. (b) LSV curve of CoO_x/Co/C-800. (c) Steady-state PL spectra of $[Ru(bpy)_3]Cl_2$, $[Ru(bpy)_3]Cl_2+Na_2S_2O_8$ and $[Ru(bpy)_3]Cl_2$+catalyst+$Na_2S_2O_8$. (d) Time-resolved PL spectra of $[Ru(bpy)_3]Cl_2$ and $[Ru(bpy)_3]Cl_2$+catalyst+$Na_2S_2O_8$. (e) Proposed mechanism of CoO_x/Co/C-800 for photocatalytic oxygen evolution.

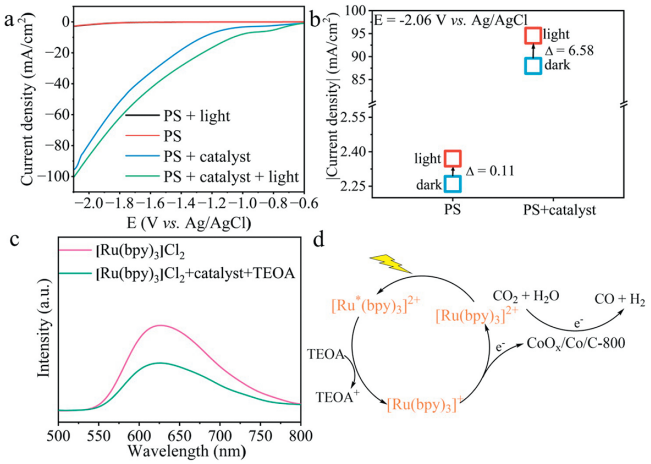

Fig. 6. (a, b) *j-V* curves of PS, PS + light, PS + catalyst and PS + catalyst + light and result. (c) Steady-state PL spectra of $[Ru(bpy)_3]Cl_2$ and $[Ru(bpy)_3]Cl_2$+catalyst+TEOA. (d) Proposed mechanism of CoO_x/Co/C-800 for photocatalytic CO_2 reduction.

Electrochemical experiments and photoluminescence spectroscopy were carried out to investigate the reaction mechanism. The half-wave potential $E_{1/2}$ of the photosensitizer representing its oxidation capacity is about 1.91 V *vs.* RHE (Fig. 5a), which is larger than onset potential of the catalyst of 1.55 V *vs.* RHE (Fig. 5b), indicating that photosensitizer can thermodynamically oxidize water [22,32]. Furthermore, the separation efficiency of photo-generated carriers was evaluated by photoluminescence (PL) spectroscopy (Fig. 5c). With the addition of sacrificing reagent, the intensity of emission peak decreases. After the addition of CoO_x/Co/C-800, the peak intensity further decreases, indicating that the catalyst promotes electron transfer and accelerates the reaction process. The fluorescence lifetime of $[Ru(bpy)_3]Cl_2$+CoO_x/Co/C-800+$Na_2S_2O_8$ is 297 ns, which is shorter than that of $[Ru(bpy)_3]Cl_2$ with 351 ns (Fig. 5d), indicating a faster completion of catalytic reactions [38,39].

Water oxidation mechanism over CoO_x/Co/C-800 is proposed as Fig. 5e. When light is illuminated, $[Ru(bpy)_3]^{2+}$ absorbs photons and changes into an excited state of $[Ru(bpy)_3]^{2+*}$. Photogenerated oxidant $[Ru(bpy)_3]^{3+}$ is formed through the $[Ru(bpy)_3]^{2+*}$ transfer electrons to $S_2O_8^{2-}$. After that, $[Ru(bpy)_3]^{3+}$ oxidizes the catalyst to high valence cobalt species and then oxidizes the water to oxygen [40,41].

The light-assisted linear sweep voltammetry curves (*j-V*) are illustrated in Fig. 6a. When illuminated, the current of both systems will increase due to the photogenerated carriers. When catalyst CoO_x/Co/C-800 was fabricated as working electrode, the current density is significantly higher than that of only photosensitizer. As shown in Fig. 6b, compared to dark condition, an increase in current corresponding to a rapid transfer of carriers between the catalyst and the photosensitizer after illuminating is found [42,43]. At the same potential, the change of current density of photosensitizer before and after illumination is 0.11 mA/cm^2, while for photosensitizer+CoO_x/Co/C-800 system, change of current density is 6.58 mA/cm^2. The increased current change value illustrates that CoO_x/Co/C-800 promotes the carrier separation of photosensitizer. For PL spectra (Fig. 6c), photosensitizer alone has a relatively high emission peak, while decreases after the addition of sacrificial reagent and CoO_x/Co/C-800, suggesting that the catalyst has the ability to rapidly transfer electrons from the excited state photosensitizer [38].

A mechanism about photocatalytic CO_2 reduction over CoO_x/Co/C-800 is shown in Fig. 6d. Photosensitizer $[Ru(bpy)_3]^{2+}$ turns into an excited state $[Ru(bpy)_3]^{2+*}$ under visible light and then is quenched by TEOA to form the reduced state $[Ru(bpy)_3]^{+}$. An electron is then transferred from $[Ru(bpy)_3]^{+}$ to the catalyst CoO_x/Co/C-800, where the adsorbed CO_2 molecules obtain electrons and is reduced to CO [44,45].

In conclusion, a series of catalysts were prepared by calcination of Co-EDTA for photocatalytic water oxidation and CO_2 reduction reactions. Among them, CoO_x/Co/C-800 obtained by calcinating Co-EDTA under N_2 and air atmosphere in sequence gives the best photocatalytic activity for both oxygen evolution and CO_2 reduction reaction. For the oxygen evolution reaction, CoO_x/Co/C-800 obtained by two-step calcination has a better catalytic activity than Co/C-800, which may be ascribed to the formation of high-valence oxidized intermediate species. In the photocatalytic CO_2 reduction reaction, CoO_x/Co/C-800 shows better CO selectivity than that of Co/C-800 due to the existence of active species inactive to hydrogen evolution. These results indicate fabricating more surface hypervalent species is not only a good method to enhance oxygen production activity, but also promote the selectivity of CO_2 reduction reaction by inhibiting hydrogen production activity. Overall, this work provides a reference for designing suitable catalysts possessing the both capacity for water oxidation and CO_2 reduction and it provides a possibility to realize artificial photosynthesis.

Declaration of competing interest

The authors declare that they have no known competing financial interests or personal relationships that could have appeared to influence the work reported in this paper.

Acknowledgments

This work was financially supported by the National Natural Science Foundation of China (No. 22075119) and the Natural Science Foundation of Gansu Province (No. 21JR7RA440).

Supplementary materials

Supplementary material associated with this article can be found, in the online version, at doi:10.1016/j.cclet.2023.108801.

References

[1] M.D. Karkas, O. Verho, E. Johnston, et al., Chem. Rev. 114 (2014) 11863–12001.
[2] D. Shindell, C. Smith, Nature 573 (2019) 408–411.
[3] J. Barber, Chem. Soc. Rev. 38 (2009) 185–196.
[4] H. Wu, X. Li, C. Tung, et al., Chem. Commun. 56 (2020) 15496–15512.
[5] J. Blakemore, R. Crabtree, G. Brudvig, Chem. Rev. 115 (2015) 12974–13005.
[6] Y. Wang, C. Zhang, R. Li, Trans. Tianjin Univ. 28 (2022) 227–235.
[7] Y. Wang, R. Liu, M. Shi, et al., Chin. Chem. Lett. 34 (2023) 107200.
[8] H. Zhang, W. Tian, X. Duan, et al., Adv. Mater. 32 (2020) 1904037.
[9] H. Takeda, C. Cometto, O. Ishitani, et al., ACS Catal. 7 (2017) 70–88.
[10] Q. Yin, J. Tan, C. Besson, et al., Science 328 (2010) 342–345.
[11] X. Meng, R. Li, J. Yang, et al., Chin. J. Catal. 43 (2022) 2414–2424.
[12] L. Wang, J. Wan, Y. Zhao, et al., J. Am. Chem. Soc. 141 (2019) 2238–2241.
[13] J. Zhang, Y. Wang, H. Wang, et al., Chin. Chem. Lett. 33 (2022) 2065–2068.
[14] L. Zhang, S. Li, H. Liu, et al., Inorg. Chem. 59 (2020) 17464–17472.
[15] W. Sun, J. Zhu, M. Zhang, et al., Chin. J. Catal. 43 (2022) 2273–2300.
[16] M. Kandy, Sustain. Energ. Fuels 4 (2020) 469–484.
[17] J. Wang, J. Jiang, F. Li, et al., Green Chem. 25 (2023) 32–58.
[18] K. Zhang, J. Ran, B. Zhu, et al., Small 14 (2018) 1801705.
[19] M. Ma, J. Chen, Z. Huang, et al., Chem. Eng. J. 444 (2022) 136585.
[20] Q. Zhang, W. Xu, C. Han, et al., Carbon 126 (2018) 128–134.
[21] S. Qiao, J. Guo, D. Wang, et al., Int. J. Hydrog. Energy 45 (2020) 1629–1639.
[22] M. Zhang, Y. Huang, J. Wang, et al., J. Mater. Chem. A 4 (2016) 1819–1827.
[23] K. Zhao, S. Zhao, C. Gao, et al., Small 14 (2018) 1800762.
[24] X. Meng, C. Zhang, C. Dong, et al., Chem. Eng. J. 389 (2020) 124432.
[25] M.A. Pimenta, G. Dresselhaus, M. Dresselhaus, et al., Phys. Chem. Chem. Phys. 9 (2007) 1276–1291.
[26] J. Guan, C. Ding, R. Chen, et al., Chem. Sci. 8 (2017) 6111–6116.
[27] S. Hsu, S. Hung, H. Wang, et al., Small Methods 2 (2018) 1800001.
[28] P. Menezes, A. Indra, D. Gonzalez-Flores, et al., ACS Catal. 5 (2015) 2017–2027.
[29] X. Li, R. Zhu, Mater. Adv. 3 (2022) 3885.
[30] F. Song, Y. Ding, B. Ma, et al., Energy Environ. Sci. 6 (2013) 1170–1184.
[31] A. Indra, P. Menezes, I. Zaharieva, et al., Angew. Chem. Int. Ed. 52 (2013) 13206–13210.
[32] M. Zheng, Y. Ding, L. Yu, et al., Adv. Funct. Mater. 27 (2017) 1605846.
[33] Q. Zhai, S. Xie, W. Fan, et al., Angew. Chem. Int. Ed. 52 (2013) 5776–5779.
[34] Y. Dou, A. Zhou, Y. Yao, et al., Appl. Catal. B 286 (2021) 119876.
[35] Z. Guo, S. Cheng, C. Cometto, et al., J. Am. Chem. Soc. 138 (2016) 9413–9416.
[36] S. Wang, Y. Zhang, Y. Zheng, et al., Small 19 (2023) 2204774.
[37] Y. Xi, W. Mo, Z. Fan, et al., J. Mater. Chem. A 10 (2022) 20934.
[38] L. Tan, S. Xu, Z. Wang, et al., Angew. Chem. Int. Ed. 58 (2019) 11860–11867.
[39] W. Sun, Y. Dong, X. Zhai, et al., Chem. Eng. J. 430 (2022) 132872.
[40] Y. Dong, T. Tian, C. Xu, et al., J. Catal. 382 (2020) 13–21.
[41] J. Lin, X. Meng, M. Zhen, et al., Appl. Catal. B 241 (2019) 351–358.
[42] X. Meng, J. Yang, S. Xu, et al., Chem. Eng. J. 410 (2021) 128339.
[43] L. Zou, R. Sa, H. Zhong, et al., ACS Catal. 12 (2022) 3550–3557.
[44] X. Meng, J. Yang, C. Zhang, et al., ACS Catal. 12 (2022) 89–100.
[45] Z. Du, Y. Xue, X. Liu, et al., J. Mater. Chem. A 10 (2022) 3469–3477.